NJC

Accepted Manuscript

This is an *Accepted Manuscript*, which has been through the Royal Society of Chemistry peer review process and has been accepted for publication.

Accepted Manuscripts are published online shortly after acceptance, before technical editing, formatting and proof reading. Using this free service, authors can make their results available to the community, in citable form, before we publish the edited article. We will replace this *Accepted Manuscript* with the edited and formatted *Advance Article* as soon as it is available.

You can find more information about *Accepted Manuscripts* in the Information for Authors.

Please note that technical editing may introduce minor changes to the text and/or graphics, which may alter content. The journal's standard Terms & Conditions and the Ethical guidelines still apply. In no event shall the Royal Society of Chemistry be held responsible for any errors or omissions in this *Accepted Manuscript* or any consequences arising from the use of any information it contains.

ROYAL SOCIETY OF CHEMISTRY

www.rsc.org/njc

Journal Name

ARTICLE

Photodegradation of Rhodamine B over a novel photocatalyst of feather keratin decorated CdS under visible light irradiation

Received 00th January 20xx,
Accepted 00th January 20xx

DOI: 10.1039/x0xx00000x

www.rsc.org/

Qizhao Wang,*[a] Juhong Lian,[a] Qiong Ma,[a] Yan Bai,[a] Jinhui Tong,[a] Junbo Zhong,[c] Rongmin Wang, [a] Haohao Huang,*[b] and Bitao Su[a]

A novel photocatalyst of feather keratin (FK) decorated CdS is synthesized by a simple co-precipitation method. The scanning electron microscopy (SEM) observation shows that the the particle sizes of FK/CdS nanocomposites are smaller than pure CdS. It is further confirmed by Fourier transform infrared (FT-IR) spectra and X-ray photoelectron spectroscopic study (XPS) that FK and CdS coexist in the photocatalysts. The results of photocatalytic experiments demonstrate that the FK/CdS composites exhibit a significantly enhanced photocatalytic activity for the photocatalytic degradation of RhB compared with pure CdS under visible light irradiation. The enhanced photocatalytic activity of the FK/CdS composites can be attributed to the similar affinity between FK and RhB, which can effectively separate photogenerated electron-hole pairs. This method not only improves the photocatalytic activity of CdS, and also reduces the environmental pollution of waste feathers. In addition, the possible degradation mechanism of RhB is proposed.

1. Introduction

With the expanding global population and industrialization, environmental pollution becomes a global problem, and gives threat to the life of human beings. Organic dyes are common commercial chemical products that often bring about unique environmental problems[1, 2]. The largest discharge of dyes into the environment occurs via the dye effluents from textile mills and food industry, which can give rise to an acute problem for municipal waste treatment facilities. Therefore, the control against dye wastewater pollution is an important issue to be tackled. A series of solutions have been put forward to protect the human from dye wastewater. Technologies involving physical or biological treatments[3] often cannot efficiently degrade organic dye pollutant. However, photo-degradation provides an important degradation pathway in recent years. Semiconductor photocatalysis, an alternative treatment strategy, is found to successfully oxidize notorious organic dye pollutants present in wastewater[4].

CdS, an important II–VI semiconductor, has been attracting increasing attention as a visible-light catalyst due to its narrow band gap at 2.42 eV[5, 6]. Therefore, many nanostructured CdS-based materials have been used in the photocatalytic removal of dyes in waste water because of their photochemical properties. These materials include metals doped CdS (Ag[7], Cd[8] and Ni[9] doped CdS) and several CdS-containing semiconductor composites (CdS/Bi_2S_3[10] and $NaNbO_3$/CdS[11]). Nevertheless, CdS has some disadvantages

[a] College of Chemistry and Chemical Engineering, Key Laboratory of Eco-Environment-Related Polymer Materials, Ministry of Education of China, Northwest Normal University, Lanzhou 730070, China
[b] College of Materials Science and Engineering, South China University of Technology, Guangzhou, 510640, China
[c] Key Laboratory of Green Catalysis of Sichuan Institutes of High Education Institutes of Sichuan, College of Chemistry and Pharmaceutical Engineering,Sichuan University of Science and Engineering , Zigong, 643000, China
*Corresponding auther. Tel: +86 931 7972677; Fax: +86 931 7975521.
E-mail addresses: wangqizhao@163.com; qizhaosjtu@gmail.com(Q. Wang)
scuthhh@hotmail.com (H. Huang)
† Electronic Supplementary Information (ESI) available: [additional figures as mentioned in the text]. See DOI: 10.1039/x0xx00000x

as a photocatalytic material. For example, the photocatalytic efficiency of CdS is severely restricted by the fast recombination of photoexcited charge carriers[12]. In addition, CdS alone is prone to photocorrosion in aqueous solution via oxidation by photogenerated holes during the photocatalytic reaction[13]. To solve these problems, a few approaches have been developed, for instance, coupling CdS with another semiconductor (TiO_2[14], g-C_3N_4[15], etc.) or noble metal can effectively accelerate the separation and transfer of photogenerated carriers. Besides, reducing the size of CdS nanoparticles also accelerates the separation. Removing photogenerated holes away from the valence band of CdS can solve the photocorrosion problem.

Recently, the biomolecule-assisted-synthesis method has given a new and promising focus in the preparation of various nanomaterials[16]. In this paper, we report, for the first time, a facile natural polymer feather keratin assisted method for synthesizing high efficient photocatalyst CdS. Among many biomolecules, we select the feather keratin as a complex agent because of the strong complexation of sulfydryl (-SH) from reduced feather keratin and its availability. Meanwhile, there is a synergic effect between sulfydryl (-SH) of FK and the positive holes (h^+) of CdS nanoparticles to inhibit the recombination of photogenerated electron and hole pairs and to enhance the photocatalytic activity of CdS. Interestingly, lone pair electrons of sulfydryl (-SH) can draw the photogenerated holes of CdS, so the introduction of feather keratin into the system can avoid the photocorrosion problem of CdS. In our work, we demonstrate that the FK/CdS nanocomposites have higher photocatalytic activity for the photocatalytic degradation of RhB under visible-light irradiation than pure CdS. RhB is a highly photostable dye consisting of a central xanthene ring connected to four N-ethyl groups, two on each side. The photocatalytic mechanism for RhB degradation is also proposed. This method is green, low-cost, and easy for the fabrication of semiconductor nanoparticles with natural polymer, having a good application prospect.

2. Experimental section

2.1 Materials and methods

White chicken feathers were collected at a local poultry farm in Gansu Province, China. All the chemicals used in the experiments were of analytical grade and were purchased from Sinopharm chemical Reagent Co., Ltd.

2.2 Extraction of keratin from feathers (FK)

Feather keratin (FK) was extracted under reducing conditions with the so-called Shindai method. The process of extraction included three steps: ethanol pretreatment, hydrochloric acid pretreatment, and 2-mercapto-ethanol deoxidization. First, raw feathers were washed 3 times with water to remove sand and dust. Then, they were dried and were cut into small filaments with lengths of 1-2 mm. 20 g of clean feathers were refluxed in 1400 mL EtOH–H_2O for 2 h at 40 ^oC. Then they were pretreated with HCl solution at 40 ^oC for 2 h to remove grease. The ethanol and HCl were filtered off and the clean pretreated feathers were stored at room temperature. Afterwards, the pretreated feathers were immersed in 300 mL solution containing urea (6 g), sodium dodecyl sulfonate (SDS 4.8 g), 2-mercaptoethanol (2 mL) and tris (0.6 g). The mixture was stirred at 70 ^oC for 2 h under a N_2 atmosphere. After being

filtered, a keratin solution was obtained. The solution was acidified to pH=4, and the keratin was precipitated with ethanol. Subsequently, the keratin sedimentation was lyophilized for 24 h.

2.3 Synthesis of FK/CdS photocatalysts

First, 0.02 g, 0.04 g, 0.06 g, 0.08 g, 0.1 g of extracted FK were dispersed respectively in 10 mL 2 mol/L urea solution at 65 ^{o}C for 30 min to obtain the solution of soluble feather keratin, and then 0.004 g of dithiothreitol (DTT) was added to reduce disulfide bond (S-S) in feather keratin to get sulfydryl (-SH) and to make feather keratin dissolve better. An aqueous solution of $Cd(Ac)_2 \cdot 2H_2O$ (20 mL, 0.01 M) was added slowly to the feather keratin solutions under vigorous stirring, then , stirring for 30 min. Afterwards, Na_2S (20 mL, 0.01 M) aqueous solution was added dropwise to the above mixture, followed by sonication for 20 min. The yellow mixtures were then stirred at 80 □ for 8 h. The weight ratios of FK to CdS in the mixtures were 1.4%, 2.7%, 4.0%, 5.3%, 6.5%, respectively. The samples were centrifuged and washed five times with deionized water and ethyl alcohol, and then were dried in an oven at 80 ^{o}C for 12 h. By contrast, CdS nanoparticles were synthesized by the same method without feather keratin.

2.4 Measurement of photocatalytic activity

The photocatalytic activity of FK/CdS photocatalysts was evaluated by degradation efficiency of RhB. Photocatalytic reaction was performed in a quartz tube reactor. 0.1 g photocatalyst was dispersed in RhB aqueous solution (50 mL, 20 mg/L). The suspensions were magnetically stirred in dark for 20 min in order to reach adsorption/desorption equilibrium of RhB molecules on the surface of photocatalysts, and then the suspensions were irradiated using a 300W Xe lamp illumination with restricted visible light radiation by a 420 nm cutoff filter. During the irradiation, about 5 mL of suspensions were continually taken from the reaction cell at 10 min intervals for subsequent target dye concentration analysis after centrifuging. The degradation efficiencies of RhB were evaluated by measuring the concentration value of the centrifuged RhB solution at 554 nm using UV-vis spectrophotometer (TU-1901, Beijing Pgeneral).

2.5 Characterization of the photocatalysts

X-ray diffraction patterns (XRD) of the prepared samples were recorded on a Rigaku X-ray diffractometer D/MAX-2200/PC equipped with Cu Ka radiation (40 kV, 20 mA). UV–vis Diffuse Reflectance spectroscopy (DRS) of powder samples was carried out at room temperature using a Shimadzu Model 3100 UV–vis spectrophotometer over a wavelength range of 200-800 nm. The reflectance spectra were transformed to absorption intensity by using Kubelka–Munk method. The surface morphology of products was observed using JSM-6701F Scanning electron microscopy (SEM) images. The structural information of the samples was measured by Fourier transform spectrophotometer (FT-IR, Vertex 70, Bruker) with KBr as the reference sample. XPS measurement was recorded on PHI5702 photoelectron spectrometer. Binding energy was referred to C1s (284.80 eV). Nitrogen adsorption–desorption isotherms and the Brunauer–Emmett–Teller (BET) surface areas were collected at 77 K on a TriStar II 3020 system. Steady and time-resolved photoluminescence (PL) spectra of samples were recorded at room temperature under 325 nm excitation

wavelength with a fluorescence spectrophotometer (PE, LS-55).

2.6 Photoelectrochemical measurements

The photocurrent of the photocatalysts was measured by electrochemical work station (CHI 650E Chenhua, Shanghai, China) in a standard three-electrode system with the as-prepared samples as the working electrodes having an active area of ca. 1.0 cm^2. Pt electrode and Ag/AgCl electrode were used as the counter and reference electrodes, respectively. A 300 W Xe lamp (Aulight, CEL-HXF 300) is used as a light source which was equipped with an optical filter (0.1 M $NaNO_2$ aqueous solution) to cut off the light in the UV region. The electrolyte solution used for all measurements was 0.5 M Na_2SO_4. For the preparation of the working electrodes, the prepared samples were dispersed ultrasonically in absolute ethanol with a concentration of 1.0 g/L. Ten drops of the suspension were put onto a piece of transparent FTO conducting glass (1×1 cm^2) and then were dried slowly at room temperature until a layer of film formed on the surface. The photocurrent responses of the working electrodes were recorded by sudden light on and off under visible light illumination at the bias voltage of 0.5 V.

3. Results and discussion

3.1 Characterization of different FK/CdS samples

XRD patterns were recorded for the dried CdS powder to confirm the crystallographic phase of CdS in the composites and examine the influence of FK on the crystallinity of CdS nanoparticles. Fig. 1 displays the XRD patterns of the FK/CdS photocatalysts with various FK/CdS weight ratios. It verifies that all the nanoparticles can be described as the cubic CdS (JCPDS card No. 65-2887). The peaks of the CdS samples correspond to the (111), (220) and (311) planes of the cubic CdS, which is in agreement with the previous report[17]. Because the content of FK is very low, no characteristic diffraction peaks arising from possible impurities are detected. The crystal phases of the FK/CdS photocatalysts are similar to that of pure CdS under the same temperature, the peak intensities of the FK/CdS decrease slightly upon enhancing the FK contents. It could be ascribed to the decreased size of the FK/CdS nanoparticles, which is consistent with scanning electron microscopy images.

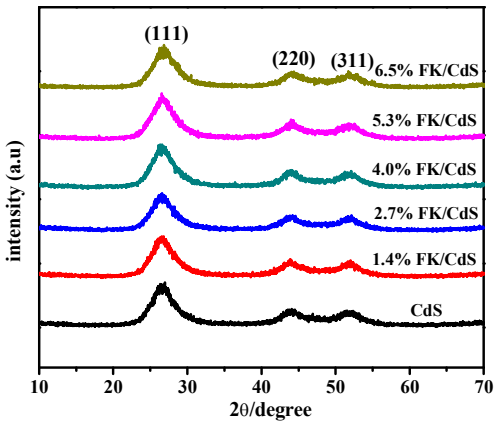

Fig. 1 XRD patterns of the as-synthesized FK/CdS nanoparticles with different FK in the CdS: pure CdS; 1.4% FK/CdS (0.02 g FK); 2.7% FK/CdS (0.04 g FK); 4.0% FK/CdS (0.06 g FK); 5.3% FK/CdS (0.08 g FK) and 6.5% FK/CdS (0.1 g FK).

UV-vis analysis is an efficient method to study optical properties of materials. The UV-vis diffuse reflectance spectra of the samples with various amounts of FK were shown in Fig. S1a. The absorption edges of various FK/CdS are all at ca.520 nm, which is in the visible light region, corresponding to the band gap of 2.4 eV. As shown in Fig. S1a, a little red-shift of the absorption spectrum is observed with increasing the content of FK. Additionally, compared to pure CdS, the absorption intensity of FK/CdS photocatalysts slightly increases in the visible-light region ranging from 420 to 500 nm. The band gap values were given in Fig. S1b, which are estimated from the intersection of the extrapolated linear portion of the curve of $(\alpha h\nu)^{1/2}$ versus photon energy. According to the eq. (1), the band gap energy of pure CdS and 4.0% FK/CdS are 2.4 eV and 2.38 eV, respectively. The introduction of FK extends the absorption of visible-light and enhances the utilization of visible-light. Therefore, it is inferred that the FK/CdS composites might possess higher photocatalytic activity than pure CdS under visible-light irradiation.

$$Eg(eV)=1240nm/\lambda(nm) \quad (1)$$

where Eg stands for the band gap energy, and λ stands for the light absorbance edge[18].

The scanning electron microscopy (SEM) has been utilized to analyze the morphology of FK/CdS nanocomposites. According to our work, the optimum weight ratio of FK to achieve the highest photocatalytic activity is 4.0% (0.06 g). Therefore, 4.0% FK/CdS is chosen as the reference sample. As displayed in Fig. 2a, large CdS nanosized particles aggregate. The size of pure CdS particles can be estimated as 150-200 nm. It is obvious that the introduction of FK has significant influence on the morphology of CdS nanoparticles. As shown in Fig. 2b, with the addition of 4.0% FK, the size of CdS particles reduces to 60-100 nm. Moreover, there exist some nanosheets. The formation of sulfydryl (-SH) of feather keratin is the main factor of decreased nanoparticles. The sulfydryl captures Cd ions to form FK-Cd (II) complex (Fig. S2) and prevents the agglomeration of CdS by releasing cadmium ions slowly into the solution. It has been reported that for photocatalysts with small particles or nanoporous structures[19], the distance that the photogenerated electrons and holes have to migrate to the reaction sites on the surface shortens, which benefits the suppression of the electron/hole recombination. Fig. 2c presents that the feather keratin has a cross-linked network structure.

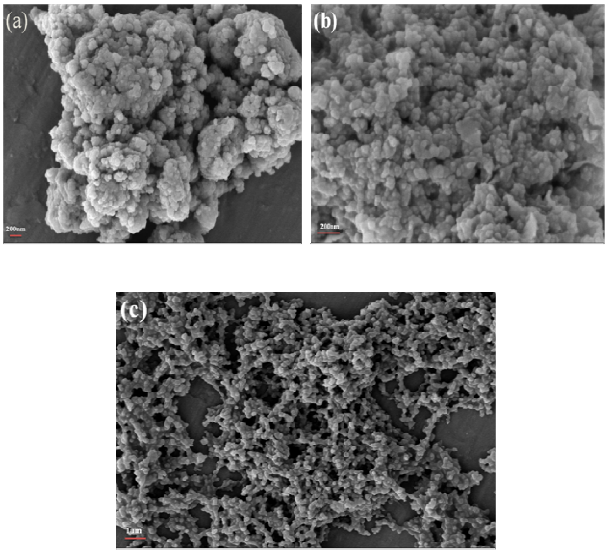

Fig. 2 SEM images of pure CdS (a), 4.0% FK/CdS (b) sample, and FK sample (c)

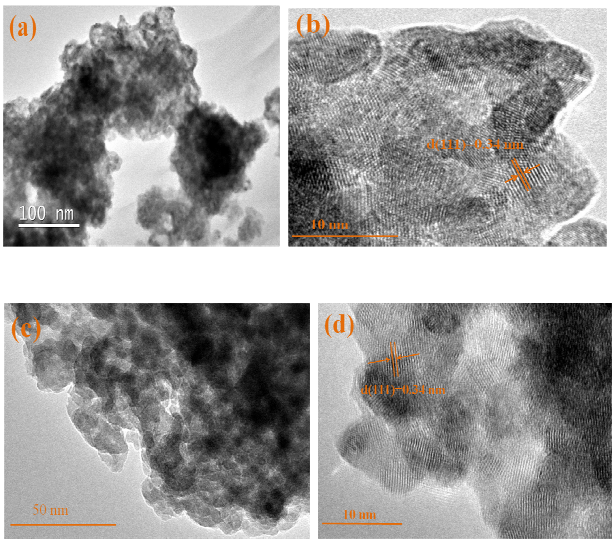

Fig. 3 TEM images of pure CdS (a) and 4.0% FK/CdS (c) samples, and HRTEM images of pure CdS (b) and 4.0% FK/CdS samples (d).

The detailed structural information about the 4.0% FK/CdS sample is further investigated by TEM and HRTEM. From the Fig. 3a and Fig. 3c, we can find that the morphology of 4.0% FK/CdS is similar with pure CdS, both of them are agglomerated nanoparticles, but the 4.0% FK/CdS sample shows smaller particle sizes, which is consistent with the SEM images. The HRTEM images recorded from the region of the two samples are shown in Fig. 3b and Fig. 3d. The spacing of the adjacent lattice fringes of the two samples is about 0.34nm, which is consistent with the (111) lattice planes of cubic CdS.

Fig. 4 shows the FT-IR spectra of FK, 4.0% FK/CdS and CdS photocatalysts. In the FT-IR spectra of the feather keratin (FK), the characteristic absorption peaks near 1647, 1539 and 1240 cm^{-1}, are assigned to the peptide bonds (–CONH–) that originated from bands known as amide I, amide II, and amide III, respectively. Amide I is useful in the analysis of the proteins and is mainly related to C=O stretching vibration occurring in the range 1700-1600 cm^{-1}. Amide II, which falls in the 1540-1520 cm^{-1} range, is related to N–H bending vibration. Amide III occurs in the range 1220-1300 cm^{-1}, resulting from C–N stretching and the C=O bending vibration. The positions of these bands match the previously reported values[20, 21]. Except for the sulfydryl (-SH), feather keratin has a good chelating ability with transition metal ions because of the presence of these groups. Therefore, Cd ion complexes of feather keratin can be used as precursors for synthesizing CdS composites. For CdS, the broad band centered at 3437 cm^{-1} and 1627 cm^{-1} are contributed to the surface adsorption of water molecules. The characteristic bands at 1381 and 1158 cm^{-1} can be attributed to the Cd-S bond[22]. For 4.0% FK/CdS photocatalyst, all the FT-IR characteristic bands of FK and CdS are also identified, confirming that the composite photocatalyst is composed of FK and CdS.

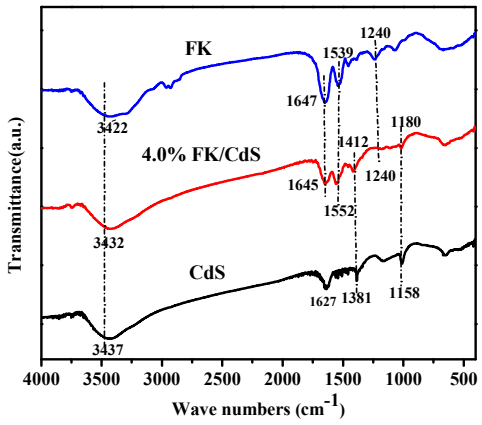

Fig. 4 FT-IR spectra of FK, 4.0% FK/CdS and CdS photocatalysts.

The chemical compositions of the as-obtained 4.0% FK/CdS sample were further analyzed by X-ray photoelectron spectra (XPS). Fig. S3a shows the representative XPS survey spectra of the 4.0% FK/CdS sample, which clearly demonstrates the existence of C, O, Cd and S elements. Fig. S3b shows the high-resolution XPS spectrum of Cd3d for 4.0% FK/CdS. The binding energies corresponding to $Cd3d_{5/2}$ and $Cd3d_{3/2}$ are 405.3 and 411.9 eV, respectively, indicative of Cd^{2+} in CdS. The splitting energy of 6.6 eV between the binding energies of Cd $3d_{5/2}$ and Cd $3d_{3/2}$ peaks is also characteristic of Cd^{2+} in CdS[23]. The binding energy of S 2p is identified at 161.8 eV, as depicted in Fig. S3c, which is consistent with the previous reported values for CdS[24]. As shown in Fig. S3d, the high-resolution C 1s XPS spectrum of 4.0% FK/CdS can be fitted into two peaks at 284.8 and 288.1 eV, corresponding to C atoms in different functional groups C-C and C=O bonds, respectively. Besides, the N1s peak is also observed (Fig. S3e), which should be ascribed to the amine group in the keratin as generally known. This indicates that the presence of FK and CdS in the 4.0% FK/CdS composites, which consists with the FT-IR spectra.

The BET surface area and pore structure of the 4.0% FK/CdS, 5.3% FK/CdS composites and pure CdS samples were investigated using nitrogen adsorption–desorption measurements (Fig. S4). The isotherms of these samples have two hysteresis loops, indicating bimodal pore-size distributions in the mesoporous (2-50 nm) and macroporous (>50 nm) regions. For the 4.0% FK/CdS and pure CdS, in low P/P_0 range ($0.5 < P/P_0 < 0.8$), the hysteresis loop is of type H2, while, for the 5.3% FK/CdS, the low P/P_0 range is $0.3 < P/P_0 < 0.5$, suggesting the presence of ink-bottle pores. In high P/P_0 range ($0.8 < P/P_0 < 1.0$), the shape of hysteresis loop is of type H3, associated with narrow slit-shaped pores. The isotherms for the 4.0% FK/CdS and 5.3% FK/CdS samples show high adsorption at relative pressures (P/P_0) approaching 1.0, suggesting the formation of macropores. Such organized porous structures might be useful in photocatalysis because they provide efficient transport pathways for reactant and product molecules[25]. The BET surface areas of 4.0% FK/CdS and 5.3% FK/CdS are found to be 94 m^2g^{-1} and 79 m^2g^{-1}, which are much lower than the value of the pure CdS sample (133 m^2g^{-1}). This occurs due to the aggregation of small particles of 4.0% FK/CdS and 5.3% FK/CdS samples. The pore size distribution curves (inset in Fig. S4) of the samples show a wide pore size distribution, further proving the presence of mesoporous and macroporous.

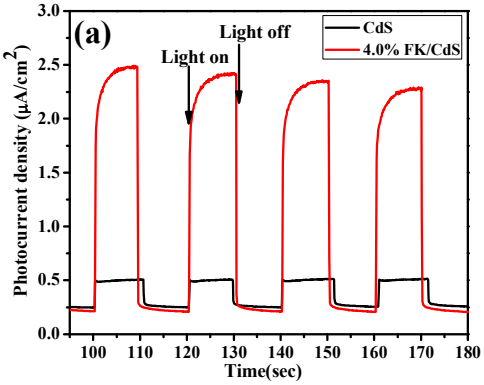

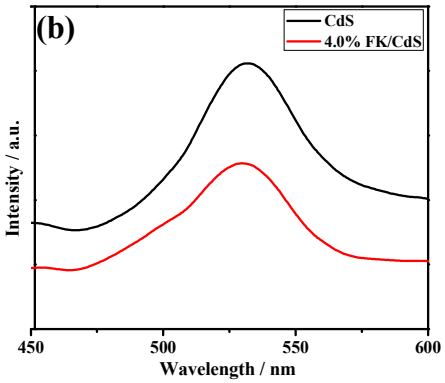

Fig. 5 The transient photocurrent of pure CdS and 4.0% FK/CdS samples under visible light (a); The photoluminescence (PL) spectra of pure CdS and 4.0% FK/CdS nanocomposites with the excitation wavelength of 325 nm (b).

The photocurrent measurement is used to reflect the interface charge separation efficiency and higher photocurrent intensity often leads to better photocatalytic activity. Fig. 5a shows the photoresponses of the 4.0% FK/CdS and pure CdS samples under visible light irradiation. When the visible light is regularly switched on and off every ten seconds, a series of almost identical electric signals could be detected and the photocurrent is maintained stably. The pure CdS shows a low photocurrent density of 0.25 μA/cm^2, whereas the value for the 4.0% FK/CdS CdS is 2.25 μA/cm^2, which is 9 times higher than that of pure CdS. This significant enhancement of the photocurrent indicates a smaller recombination and more efficient separation of photogenerated electron–hole pairs at the 4.0% FK/CdS interface: the lone pair electrons of sulfydryl (-SH) can draw the photogenerated holes of CdS, thus efficiently inhibiting the recombination of photogenerated electron and hole pairs of CdS and prolonging the lifetime of charge carriers. The smaller size of 4.0% FK/CdS nanoparticles than pure CdS is also beneficial for separation of photogenerated electron-hole pair.

Since photoluminescence (PL) emission mainly arises from the recombination of free carriers, PL spectroscopy is a facile technique to survey the separation efficiency of photoinduced electron–hole pairs in a semiconductor[26]. Fig. 5b shows the room temperature photoluminescence spectra of pure CdS and the 4.0% FK/CdS samples with an excitation wavelength of 325 nm. The pure CdS displays a strong PL emission peak centered at about 530 nm, for the 4.0% FK/CdS photocatalyst, however, the intensity of the emission peak significantly decreases, indicating the more efficient inhibition of electron–hole pairs recombination. This occurs because the distance that the photogenerated electrons and holes have to migrate to the reaction sites on the surface shortens for smaller particles or nanoporous structures[21], which benefits the suppression of the electron/hole recombination. In addition, due to the synergic effect between sulfydryl (-SH) of FK and the positive holes (h^+) of CdS nanoparticles, the photogenerated electron–hole pairs at the 4.0% FK/CdS interface can also be separated efficiently.

3.2 Photocatalytic performance and photostability

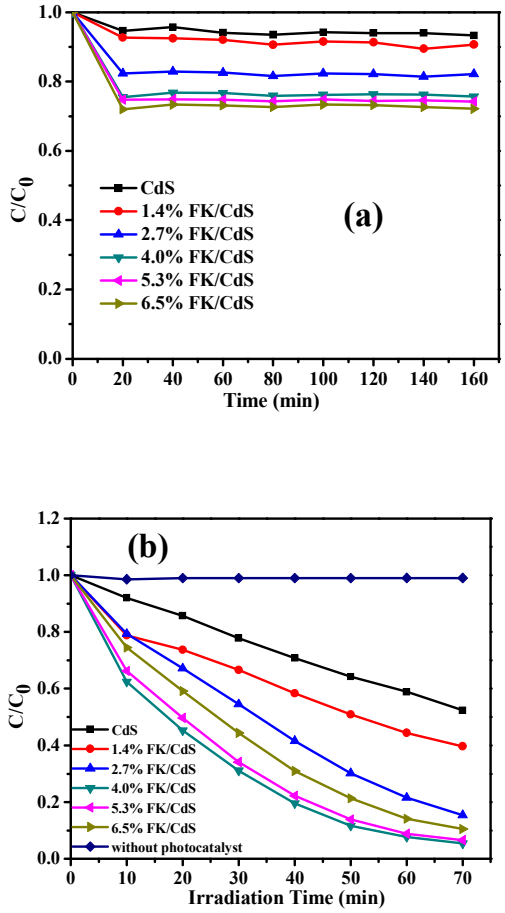

Fig. 6 The adsorption property of all the samples under darkness (a) and photodegradation efficiencies (C/C_0) of RhB as a function of irradiation time under visible light irradiation (b).

The photocatalytic activities of the as-prepared samples were evaluated by degradation of RhB under visible light radiation. The photocatalytic activities of different catalysts are given in Fig. 6. The decolorization experiments are divided into two stages, 160 min absorption stage (Fig. 6a) and 70 min photodegradation stage (Fig. 6b). From Fig. 6a, we can see that all samples have reached absorption/desorption equilibrium after 20 min. The absorption efficiency of the CdS, 1.4% FK/CdS, 2.7% FK/CdS, 4.0% FK/CdS, 5.3% FK/CdS and 6.5% FK/CdS is 5.4%, 7.3%, 17.7%, 24.5%, 25.3% and 28.1%, respectively. Fig. 6b shows the photocatalytic activity of different samples after absorption equilibrium. It can be seen that self-degradation of RhB is negligible, indicating the stabilization of RhB molecule. The FK/CdS nanocomposites show higher photocatalytic activities than pure CdS, especially for the 4.0% FK/CdS sample, which possesses the best photocatalytic activity and provides the photodegradation efficiency about 96.6% after 70 min. The high photocatalytic activity of the FK/CdS nanocomposites can be attributed to the increased charge separation of FK/CdS due to synergic effect and the smaller particles caused by FK and the similar affinity between FK and RhB. However, when excess FK is introduced, the surface of CdS is almost coated with FK, hindering the visible light absorption of CdS. Furthermore, when excess FK is introduced, the number of active sites for the degradation of organic dyes via CdS becomes few, leading to photoactivity fading.

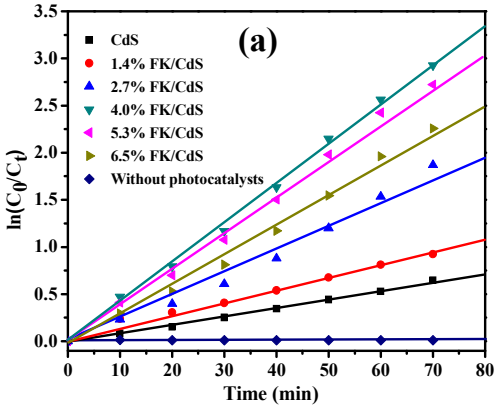

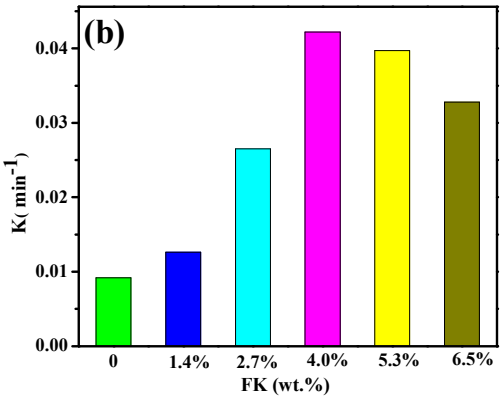

Fig. 7 The first-order kinetics plots (a) and constants (b) for photocatalytic degradation of RhB under visible light irradiation.

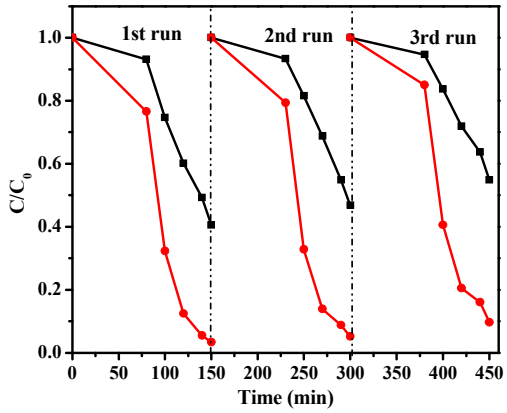

Fig. 8 Cycling runs for the photocatalytic degradation of RhB in the presence of the pure CdS (square) and 4.0% FK/CdS sample (circle).

The kinetics of the degradation reaction can be described by using a first-order model for low concentrations of RhB solutions. The pseudo first-order kinetics equation is expressed as $\ln(C_0/C_t)=k_{app}t$, where C_t is the RhB concentration in aqueous solution at time t (mg/L), C_0 is the initial RhB concentration (mg/L), and k_{app} is the apparent pseudo-first-order kinetic constant (min^{-1}). The relations between $\ln(C_0/C_t)$ and irradiation time (t) are plotted in Fig. 7a. The values of k_{app} are calculated and listed in Fig. 7b. The excellent fitting indicates that the photoreaction follows first-order reaction kinetics. From Fig. 7, it is found that the degradation rate constant of 4.0% FK/CdS is about 4.6 times higher than that of pure CdS.

The capability for reuse is one of the most important factors for photocatalysts. Hence, the reusability and stability of the 4.0% FK/CdS sample and pure CdS were investigated. The samples are collected after degradation experiments and reused three times. As shown in Fig. 8, the two samples also exhibit gradually reduced activities, for the pure CdS, only 45.2% of RhB can be removed in the third cycles, reducing about 14.2%. But for the 4.0% FK/CdS, only a slight drop of the efficiency from 96.6% to 90.3%. This represents that the 4.0% FK/CdS has better stability than pure CdS.

3.3 photocatalytic mechanism

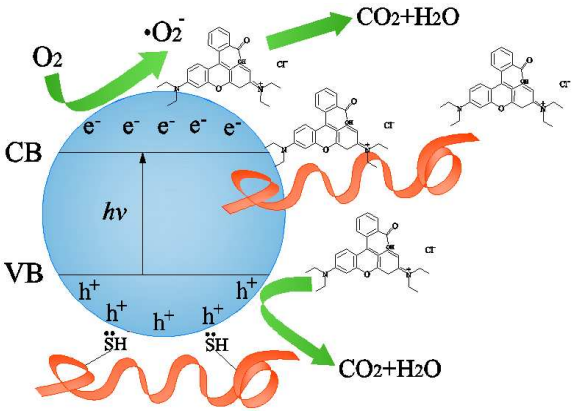

Fig. 9 The proposed mechanism for the photocatalytic degradation of RhB solution by FK/CdS nanocomposites.

To determine the photocatalytic degradation mechanism, the main photocatalytic process is illustrated in Fig. 9. The adsorption decolourisation is mainly caused by the similar affinity between FK and RhB. When FK/CdS nanoparticles are immersed into the RhB solution, some RhB molecules diffuse through the gaps among the CdS nanoparticles and reach the surface of FK because of their similar intermiscibility where they are adsorbed. After 20 min, the adsorption could almost reach the saturation. The photocatalytic decomposition of RhB molecules by CdS nanoparticles is the main factor that causes decolourisation. When CdS nanoparticles are irradiated under visible light, the electrons of the valence band (VB) are excited to the conductor band (CB), as depicted in Fig. 9. Thus, positive holes (h^+) are produced in the VB. The electrons then react with the O_2 molecules adsorbed on the surface of CdS to generate super oxide ions ($\bullet O^{2-}$) because the CB band of CdS (−0.57eV) is more negative than the standard redox potentials of $O_2/\bullet O^{2-}$ (−0.28eV)[27]. Subsequently, the RhB molecules are oxidised by $\bullet O^{2-}$ ions and are decomposed into inorganic materials (CO_2 and H_2O). However, the VB edge potential of CdS (1.68 eV) is less positive than E0 ($\bullet OH/OH^-$) (+2.38 eV)[28], confirming that the photogenerated holes could not oxidize OH− to yield •OH. So the holes can oxidate RhB into inorganic materials (CO_2 and H_2O) directly. Therefore the holes in the VB of CdS and the $\bullet O^{2-}$ radicals are beneficial for the RhB degradation[11]. Consequently, the FK/CdS nanocomposites have higher photocatalytic activity than pure CdS due to their smaller size and synergic effect between the sulfydryl group of FK and the positive holes of CdS.

4. Conclusions

In conclusion, we have successfully synthesized a novel natural biopolymer feather keratin modified CdS photocatalyst via the precipitation method. The as-prepared catalysts show much higher photocatalytic activity than pure CdS toward the degradation of RhB under visible-light irradiation. The experimental results demonstrate that the 4.0% FK/CdS photocatalyst has an optimum performance in the removal of organic pollutant RhB. The photocatalytic RhB degradation over FK/CdS follows the pseudo-first-order kinetic model. The enhanced photocatalytic activity of FK/CdS can be ascribed to the increased charge separation of FK/CdS due to synergic effect and the smaller particles caused by FK and the similar affinity between FK and RhB. Additionally, we find that the lone pair electrons of sulfydryl(-SH) can draw the photogenerated holes of CdS, so the introduction of feather keratin prevents the photocorrosion problem of CdS. The approach presented in this study is green and low-cost, not only enhancing the photocatalytic activity of CdS, and also reducing the environmental pollution of waste feathers. It

provides a wide application prospects in the fields of photocatalysis, especially in the photodegradation organic pollutants.

Acknowledgements

This work was financially supported by the National Natural Science Foundation of China (No.51262028, 21263024, 21364012), Natural Science Foundation of Gansu Province (1107RJZA194), the Opening Project of Key Laboratory of Green Catalysis of Sichuan Institutes of High Education, and the Program for Undergraduate Academic Innovative Research of Northwest Normal University.

Notes and references

1. Y. Xie, G. Ali, S. H. Yoo and S. O. Cho, *ACS applied materials & interfaces*, 2010, **2**, 2910-2914.
2. K. Vinodgopal, I. Bedja and P. V. Kamat, *Chemistry of Materials*, 1996, **8**, 2180-2187.
3. S. S, P. K, G. R, G. M. A and M. N, *Dyes and Pigments*, 2006, **69**, 22-30.
4. S. Liu, J. Yu and M. Jaroniec, *Journal of the American Chemical Society*, 2010, **132**, 11914-11916.
5. H. Liu, K. Zhang, D. Jing, G. Liu and L. Guo, *International Journal of Hydrogen Energy*, 2010, **35**, 7080-7086.
6. H. Zhu, R. Jiang, L. Xiao, Y. Chang, Y. Guan, X. Li and G. Zeng, *Journal of Hazardous Materials*, 2009, **169**, 933-940.
7. J. Ma, G. Tai and W. Guo, *Ultrasonics sonochemistry*, 2010, **17**, 534-540.
8. Y. Huang, F. Sun, H. Wang, Y. He, L. Li, Z. Huang, Q. Wu and J. C. Yu, *Journal of Materials Chemistry*, 2009, **19**, 6901-6906.
9. M. Luo, Y. Liu, J. Hu, H. Liu and J. Li, *ACS applied materials & interfaces*, 2012, **4**, 1813-1821.
10. Y. Yan, Z. Zhou, W. Li, Y. Zhu, Y. Cheng, F. Zhao and J. Zhou, *RSC Advances*, 2014, **4**, 38558.
11. S. Kumar, S. Khanchandani, M. Thirumal and A. K. Ganguli, *ACS applied materials & interfaces*, 2014, **6**, 13221-13233.
12. Y. Shi, K. Zhou, B. Wang, S. Jiang, X. Qian, Z. Gui, R. K. K. Yuen and Y. Hu, *Journal of Materials Chemistry A*, 2014, **2**, 535-544.
13. Q. Li, B. Guo, J. Yu, J. Ran, B. Zhang, H. Yan and J. R. Gong, *Journal of the American Chemical Society*, 2011, **133**, 10878-10884.
14. M. Liu, J. Zheng, Q. Liu, S. Xu, M. Wu, Q. Xue, Z. Yan, H. Xiao, Z. Wei and H. Zhu, *RSC Advances*, 2013, **3**, 9483-9489.
15. F. Jiang, T. Yan, H. Chen, A. Sun, C. Xu and X. Wang, *Applied Surface Science*, 2014, **295**, 164-172.
16. D. Ghosh, S. Mondal, S. Ghosh and A. Saha, *Journal of Materials Chemistry*, 2012, **22**, 699-706.
17. Q. Wang, J. Li, Y. Bai, X. Lu, Y. Ding, S. Yin, H. Huang, H. Ma, F. Wang and B. Su, *Journal of photochemistry and photobiology. B, Biology*, 2013, **126**, 47-54.
18. J. Sun, G. Chen, Y. Feng and Y. Wang, *RSC Adv.*, 2014, **4**, 44466-44471.
19. A. Kudo and Y. Miseki, *Chemical Society reviews*, 2009, **38**, 253-278.
20. X.-C. Yin, F.-Y. Li, Y.-F. He, Y. Wang and R.-M. Wang, *Biomaterials Science*, 2013, **1**, 528.
21. N. V. Bhat and S. M. Ahirrao, *Journal of Polymer Science: Polymer Chemistry Edition*, 1983, **21**, 1273-1280.
22. J. Fu, B. Chang, Y. Tian, F. Xi and X. Dong, *Journal of Materials Chemistry A*, 2013, **1**, 3083-3090.
23. L. Qi, J. Yu and M. Jaroniec, *Physical Chemistry Chemical Physics*, 2011, **13**, 8915-8923.
24. T. Zhai, X. Fang, Y. Bando, Q. Liao, X. Xu, H. Zeng, Y. Ma, J. Yao and D. Golberg, *ACS nano*, 2009, **3**, 949-959.
25. J. Yu, J. Jin, B. Cheng and M. Jaroniec, *Journal of Materials Chemistry A*, 2014, **2**, 3407.
26. Y. Shi, H. Li, L. Wang, W. Shen and H. Chen, *ACS applied materials & interfaces*, 2012, **4**, 4800-4806.
27. Z. Ai, W. Ho and S. Lee, *The Journal of Physical Chemistry C*, 2011, **115**, 25330-25337.
28. H. Cheng, B. Huang, Y. Dai, X. Qin and X. Zhang, *Langmuir : the ACS journal of surfaces and colloids*, 2010, **26**, 6618-6624.